Research Article | Vol. 8, No. 11 | 1 Nov 2018 | OPTICAL MATERIALS EXPRESS 3392
Optical Materials EXPRESS

Degenerate optical nonlinear enhancement in epsilon-near-zero transparent conducting oxides

ENRICO GIUSEPPE CARNEMOLLA,[1] LUCIA CASPANI,[2] CLAYTON DEVAULT,[3] MATTEO CLERICI,[4] STEFANO VEZZOLI,[5] VINCENZO BRUNO,[6] VLADIMIR M. SHALAEV,[7] DANIELE FACCIO,[6] ALEXANDRA BOLTASSEVA,[7] AND MARCELLO FERRERA[1]

[1]*Institute of Photonics and Quantum Sciences, Heriot-Watt University, SUPA, Edinburgh, Scotland, EH14 4AS, UK*
[2]*Institute of Photonics, Department of Physics, University of Strathclyde, Glasgow G1 1RD, UK*
[3]*Dept. of Physics & Astronomy and Birck Nanotechnology Center, Purdue University, West Lafayette, IN, 47907, USA*
[4]*School of Engineering, University of Glasgow, Glasgow G12 8QQ, UK*
[5]*Department of Physics, King's College London, Strand, London WCR 2LS, UK*
[6]*School of Physics and Astronomy, University of Glasgow, Glasgow G12 8QQ, UK*
[7]*School of Electrical and Computer Engineering, Purdue University, West Lafayette, IN 47907, USA*
**m.ferrera@hw.ac.uk*
www.asn-lab.org

Abstract: We report the simultaneous increase of both nonlinear Kerr coefficient n_2 and third-order nonlinear susceptibility $\chi^{(3)}$ in aluminum zinc oxide (AZO) attained by pump-probe spectroscopy in a frequency degenerate configuration. Our experiments demonstrate a 6-fold enhancement in the third-order nonlinear susceptibility and over one order of magnitude increase in the nonlinear Kerr coefficient, while also determining two distinct operational wavelengths for optimal modulation of either the real or the imaginary part of the complex refractive index. These results, besides providing a broader spectral characterization of the third-order nonlinearity in AZO thin films, also show the fundamental advantages of performing nonlinear optics via degenerate excitation near the ENZ wavelength.

1. Introduction

Over the past decade, nanophotonics research has been heavily focusing on developing and advancing material platforms for practical nanophotonic devices that are low-loss, tailorable and can easily be integrated with existing semiconductor technologies. On the direction of low-loss CMOS compatible technologies and metal-free nanophotonics, the scientific community is moving towards all-dielectric components [1], where dielectric materials replace the metallic inclusions in high refractive index contrast systems [2]. Important proofs of concept include III-V semiconductor metasurface [3], dielectric metamaterials [4,5], and multilayer nanopillars [6]. Although extremely promising, all-dielectric nano-devices do not retain many of the desirable attributes of plasmonic devices while the requirement of operating in high index-contrast systems poses further limitations to the possible combinations of usable materials. Further limitations in the material choice arise from the requirement of having high quality thin films, whose optical properties are linked to good morphological and crystallographic matching with the surrounding environment.

Transparent Conductive Oxides (TCOs) have recently emerged as favorable hybrid materials for plasmonic applications because of their unique properties stemming from a large

#340528 https://doi.org/10.1364/OME.8.003392
Journal © 2018 Received 24 Jul 2018; revised 28 Sep 2018; accepted 2 Oct 2018; published 17 Oct 2018

Optical Materials EXPRESS

intrinsic bandgap and high carrier concentrations. The latter feature pushes the Fermi level into the conduction band and widens the bandgap of the intrinsic material via the Moss-Burstein shift. Among the most exploited TCOs we find Indium Tin Oxide (ITO), Aluminum Zinc Oxide (AZO), Gallium Zinc Oxide (GZO) and Indium Cadmium Oxide (ICO). These compounds are routinely used for industrial purposes to fabricate touch-screen displays and photovoltaic systems and only recently they have become metal substitutes for plasmonic applications [7].

The use of TCOs for integrated photonic applications is also justified by their unique nonlinear properties. For instance, photoexcitation was exploited in nanostructured nonlinear systems by Guo et al. for both modulating the material absorption via interband excitation [8] and tuning the mode resonance of localized plasmons using intraband nonlinearities [9]. TCO-mediated all-optical control of plasmon mode resonances in metallic nanoantennas has also been demonstrated in [10,11], where ITO-gold systems were employed.

Following the idea of increasing optical nonlinearities even further, we notice that TCOs allow to engineer the material dielectric permittivity so that it approaches zero at fundamental operational wavelengths across the telecom band. This can be attained by altering fabrication parameters and material stoichiometry. These Epsilon-Near-Zero (ENZ) conditions bring the optical nonlinearities to unprecedented levels. In certain cases, for high pump intensity, the optically induced change in the complex refractive index can be fitted to a semi-empirical model accounting for the standard Taylor series expansion of the dielectric polarization density inclusive of higher-order nonlinear susceptibility terms up to $\chi^{(7)}$ [12–14]. These results are of fundamental interest because they might be key to overcome the typical nonlinear trade-off between magnitude and speed which has hampered the development of practical integrated nonlinear devices for decades already. TCOs, under opportune experimental conditions, can boost the typical figure of merit of nonlinear photonic devices ($FoM = n_2/\alpha$, where n_2 is the nonlinear refractive index and α represents the linear losses of the material) by 5 orders of magnitude, making this class of material a game changer in integrated photonics. In recent years, a few seminal works dealing with enhanced nonlinearities in bulk TCOs probed at ENZ wavelengths, have been published. In particular, in [15] Kinsey et al. reported ultra-fast and large interband nonlinearities in AZO thin films probed at the ENZ wavelength. An important feature of this work deals with the particular fabrication procedure developed to attain sub-picosecond recombination time [16]. More specifically, all the thin films used in our experiments have been grown by using pulsed laser deposition performed in an oxygen deprived atmosphere. The induced oxygen vacancies have the twofold effect of increasing free carriers and enlarging the number of recombination channels. The latter characteristic being responsible for shortening the photocarriers recombination time by about two orders of magnitude with respect to commercially available TCO films.

Because of the hybrid nature of TCOs being in the middle between semiconductors and metals, both interband and intraband optical nonlinearities can be efficiently excited [17,18]. These nonlinearities can be judiciously combined to increase the material bandwidth up to few THz, perform all-optical three-state logic operations, and attain ultra-fast signal routing [19]. Such large and ultrafast modulation of the material optical properties has been exploited also for efficient third harmonic generation and four-wave mixing in ITO and AZO films [20,21].

Finally, very recently, tuning metallic nano-antennas in resonance with the ENZ wavelength of an underlying TCO substrate, has been proved to be extremely effective for maximizing the effective intensity-dependent index change [22,23]. The recorded extraordinary nonlinear behavior is directly linked to a condition of “strong coupling” between the antennas and the substrate which leads to unity order refractive index change and an n_2 coefficient up to six orders of magnitude higher than the one of silica glass.

Optical Materials EXPRESS

Despite of all the remarkable results reported in literature, there is still a long way to go for a full exploration of nonlinear optics in TCO-based systems. For instance, TCOs' nonlinear optical response has been investigated only within a relatively narrow spectral window including the visible and a small fraction of the NIR range. In particular, great interest has been dedicated to the enhancement of the nonlinear refractive index due to the index-near-zero nature of the material without exploring regimes of high intrinsic third-order nonlinear susceptibility $\chi^{(3)}$. Here we present one possible strategy to further enlarge the intensity dependent refractive index change. Our approach relies on the simultaneous increase of the $\chi^{(3)}$ and of the nonlinear enhancement due to the ENZ regime. This is quite different from [17] where a flat $\chi^{(3)}$ around the cross-over wavelength allowed to define an overall nonlinear enhancement factor that is solely dependent on linear indices.

Starting from few semi-empirical models (see section 2), which link first- and third-order material susceptibilities, we gained some intuition about the general trend of the nonlinear dispersion for the simplest case of degenerate excitation. Subsequently, by means of a pump/probe set-up, where the operational wavelength is set within the ENZ material window, we proceeded with the quantitative evaluation of the predicted nonlinear enhancement.

2. Experimental analysis and methodology

The fundamental goal of our study is to assess how far we can go in increasing the nonlinear Kerr coefficient n_2 of TCOs. Establishing this limit will provide an important insight into the carrier dynamics in TCOs and will have impact on the design on novel nonlinear devices. Increase in the nonlinear effects can be attained either by acting on the third-order intrinsic nonlinear susceptibility or by exploiting the index-near-zero properties of TCOs. For instance, the nonlinear photonics community used to rely on the former approach. Here we combine the effects of both approaches. For the sake of clarity we describe in the following how n_2, $\chi^{(3)}$, and the linear refractive index n_L are linked together.

Considering a pump-probe configuration, the mathematical relation linking the nonlinear refractive index n_2 experienced by the probe beam with the third-order susceptibility $\chi^{(3)}$ (function of the pump and probe parameters) and the probe linear refractive index $n = n_r + i\, n_i$ is [24]:

$$n_2 = \frac{3}{2\varepsilon_0 c} \frac{\chi^{(3)}}{n_r^{pump}(n_r + i n_i)} \tag{1}$$

where n_2 and $\chi^{(3)}$ are also complex quantities, ε_0 is the vacuum permittivity, c is the speed of light in vacuum, $n_{r,i}$ are the real and imaginary part of the refractive index at the probe wavelength, and n_r^{pump} is the real part of the linear refractive index at the optical pump wavelength. The dependence of n_2 on $\chi^{(3)}$ implies that a straightforward tactic to increase the nonlinear response is to utilize the largest components of a material's third-order tensor $\chi^{(3)}$. This task is challenging because each tensor element will depend on both pump and probe wavelengths. To facilitate this goal, different semi-empirical methods that link the linear susceptibility $\chi^{(1)}$ to the $\chi^{(3)}$ are available in literature to predict the nonlinear properties of materials [25]. The task is further simplified if the equations are calculated for the degenerate case where all the photons involved in the parametric process have the same energy.

In Fig. 1(a), we plot the complex third-order nonlinear susceptibility $\chi^{(3)}$ as a function of the probe wavelength for three cases: i) Wang's model (dashed lines) [26]; ii) Miller's model (solid lines) [24,27]; iii) numerical evaluation of $\chi^{(3)}$ based on experimental results (+ markers). The experimental procedure to measure $\chi^{(1)}$ and $\chi^{(3)}$ will be explained later in this section.

Optical Materials EXPRESS

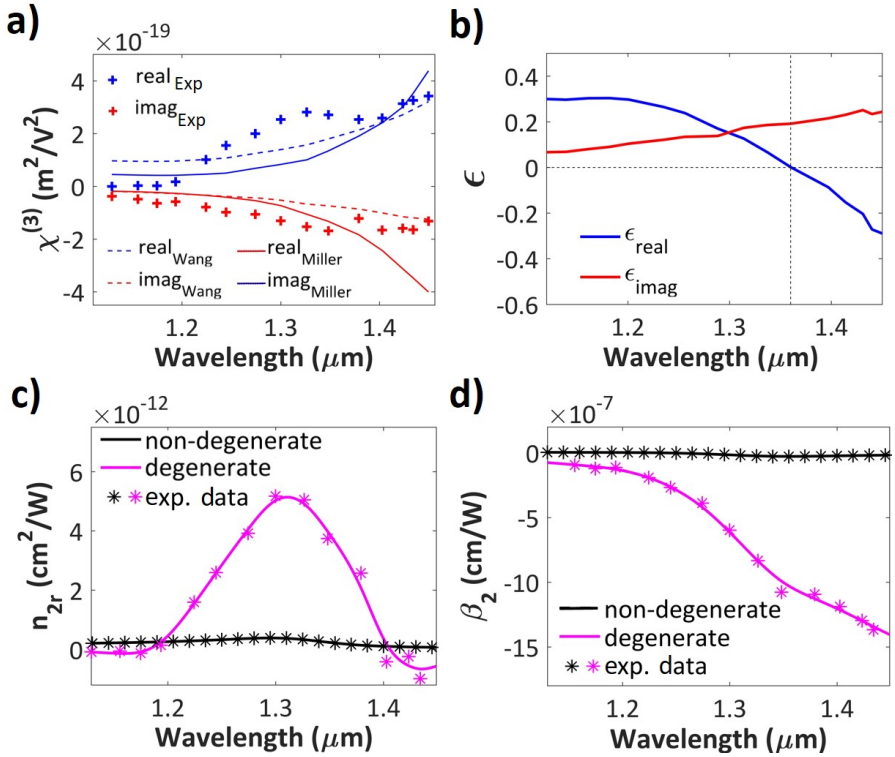

Fig. 1. (a) Real and imaginary part of the experimentally measured nonlinear susceptibility $\chi^{(3)}$ (cross points) compared with the $\chi^{(3)}$ trend obtained by the application of the Wang (dashed curves) and Miller (solid curves) relations in the wavelength range 1120 nm - 1450 nm. (b) Real (blue curve) and imaginary (red curve) part of the AZO film permittivity. The black dashed lines indicate the cross-over wavelength, which was λ_{ENZ} = 1360 nm. (c) Comparison between the nonlinear Kerr coefficient n_{2r} for the degenerate case ($\lambda_{pump} = \lambda_{probe}$, magenta line) and for the non-degenerate case (λ_{pump} = 787 nm, black line) as a function of λ_{pump} in the wavelength range 1120 nm - 1450 nm. The values of the n_{2r} are obtained using the Eq. (2). Black and magenta asterisks indicate non-degenerate and degenerate experimental data, respectively. (d) Comparison between the nonlinear absorption coefficient β_2 for the degenerate case ($\lambda_{pump} = \lambda_{probe}$, magenta line) and for the non-degenerate case (λ_{pump} = 787 nm, black line) as a function of λ_{probe} in the wavelength range 1120 nm - 1450 nm. The values of the n_{2i} are obtained using the Eq. (3) and used in the Eq. (4) to calculate the β_2. Black and magenta asterisks indicate non-degenerate and degenerate experimental data, respectively.

Both models, although being differently dependent on the linear susceptibility $\chi^{(1)}$, predict a similar monotonic behavior for both real and imaginary parts of the $\chi^{(3)}$. The same trend is also supported by our experiments. As previously mentioned, the three plots are for the case of degenerate optical excitation and they refer to a sample which exhibits cross-over wavelength at 1360 nm. Wang and Miller curves are multiplied by a factor 1×10^{-19} m^2/V^2 to be compared with the experimental evaluation of the $\chi^{(3)}$. The values of the $\chi^{(1)}$ are calculated from the simple relation $\chi^{(1)} = \varepsilon_L - 1$, where ε_L is the linear permittivity estimated following the process reported later in this section (Fig. 1(b)). The graphs, which for experimental limitation are plotted within the wavelength range 1120 nm - 1450 nm, show a clear increase of the real part of the nonlinear susceptibility $\chi_r^{(3)}$ for longer wavelengths while an almost symmetrical trend towards negative values is exhibited by the imaginary part $\chi_i^{(3)}$. Note that the two semi-empirical models are used only to predict the general trend of the $\chi^{(3)}$ dispersion without any aim at providing its quantitate evaluation. The latter task is out of reach for the impossibility in evaluating within acceptable accuracy the multiplicative constants of the empirical models (Miller's $\rightarrow \chi^{(3)} \propto [\chi^{(1)}]^4$; Wang's $\rightarrow \chi^{(3)} \propto [\chi^{(1)}]^2$).

Optical Materials EXPRESS

To combine this trend with the nonlinear enhancement at the ENZ wavelength reported by Caspani and co-authors [17], we recall the representation of the n_2 into its real (n_{2r}) and imaginary (n_{2i}) parts,

$$n_{2r} = \frac{3}{2\varepsilon_0 c}\frac{n_r\chi_r^{(3)} + n_i\chi_i^{(3)}}{D} \tag{2}$$

$$n_{2i} = \frac{3}{2\varepsilon_0 c}\frac{n_r\chi_r^{(3)} - n_i\chi_i^{(3)}}{D} \tag{3}$$

where $D = n_r^{pump}(n_r^2 + n_i^2)$. In [17] it was shown that under the condition $\chi_r^{(3)} \approx \chi_i^{(3)} \approx$const., which was adequately met for the non-degenerate case, n_{2r} and n_{2i} depend on the enhancement factors $F_r = (n_r + n_i)/D$ and $F_i = (n_r - n_i)/D$, respectively. For this case, near the ENZ wavelength λ_{ENZ}, F_r produces a peak enhancement of the n_{2r}, while n_{2i} becomes very small in absolute value thus inducing a reduction of the nonlinear absorption coefficient β_2, defined as:

$$\beta_2 = 4\pi n_{2i} / \lambda \tag{4}$$

where λ is the operational wavelength in vacuum.

For the degenerate case considered here, the condition $\chi_r^{(3)} \approx \chi_i^{(3)} \approx$const is no longer valid and the enhancement of the intensity dependent refractive index within the ENZ window is also mediated by the third-order nonlinear susceptibility. Figure 1(b) and 1(c) make a direct comparison between degenerate and non-degenerate case (λ_{pump} = 787 nm) for both real and imaginary nonlinear refractive index, respectively. These graphs illustrate how optical nonlinearities are largely enhanced by employing a degenerate pumping scheme (see *"Key findings and discussion"*). Our results prove that the degenerate optical excitation in the ENZ region is optimal to fully exploit the nonlinear capability of TCOs. The nonlinear material response was measured by using a standard pump and probe set-up in its degenerate configuration as sketched in Fig. 2. The target sample was a 900-nm thin film of oxygen-deprived aluminum zinc oxide (AZO) [15,28]. The film was grown by pulsed laser deposition (PVD Products, Inc.) using a target of AZO via a 248 nm KrF excimer laser (Lambda Physik GmbH) [29,30]. The fundamental source of our optical set-up was a Ti:Sapphire laser (λ = 787 nm) with a repetition rate of 100 Hz providing an optical pulse of ≈100 fs vertically polarized. The output was directed into an Optical Parametric Amplifier (OPA) which provided both pump and probe signals.

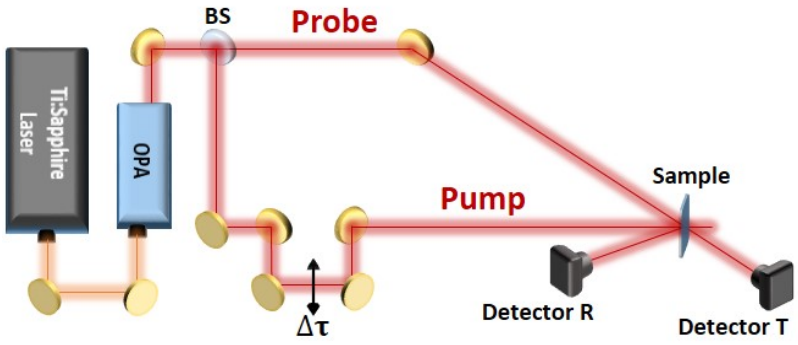

Fig. 2. Sketch of the degenerate pump and probe setup. A Ti:Sapphire laser pumps the optical parametric oscillator, whose signal is split in a high intensity pump and a weak probe, both vertically polarized and incident in the AZO sample with angle of incidence <10°.

We first measured the linear (i.e. no pump) transmission and reflection in the wavelength range between 1120 nm and 1550 nm. Then we extracted the linear permittivity ε_L by means

Optical Materials EXPRESS

of an inverse transfer matrix method (for details see [31]), finding the ENZ wavelength at λ_{ENZ} ≈1360 nm. We investigated the nonlinear properties of our AZO film by first recording both transient transmissivity and reflectivity of the probe signal as a function of the time delay $\Delta\tau$ between pump and probe. This was done for different operational wavelengths (within the range 1120 nm and 1550 nm) and for different incident pump intensities I_{pump} (within the range 20 GW/cm^2 and 90 GW/cm^2), which were corrected by subtracting the portion of the pump reflected at the interface air-AZO ($\hat{I}_{pump}$). Subsequently, the nonlinear permittivity ε_{NL} was extracted from the measurements of transmission and reflection at $\Delta\tau = 0$ by means of inverse transfer matrix method. Finally, the third-order susceptibility $\chi^{(3)}$ was calculated using the following relation:

$$\chi^{(3)}(\omega_{pump},\omega_{probe}) = \frac{n_r^{pump}\varepsilon_0 c}{3}\frac{\partial\varepsilon_{NL}(\omega_{probe},\hat{I}_{pump})}{\partial\hat{I}_{pump}} \tag{5}$$

where ω_{pump} and ω_{probe} are the pump and the probe angular frequencies, respectively, and the derivative with respect to the pump intensity is performed where $\varepsilon_{NL}(\hat{I}_{pump})$ is approximately linear [24]. The $\chi^{(3)}$ was then used to find the nonlinear Kerr coefficients n_{2r} and n_{2i} using Eq. (2) and (3), while the nonlinear absorption coefficient was calculated by Eq. (4). The values of the ε_{NL} were also used to determine the variation of the refractive index Δn, from the following relations:

$$\Delta n_{r,i} = n_{NLr,i} - n_{Lr,i} \tag{6}$$

where Δn_r and Δn_i are the real and imaginary part of Δn, respectively. The terms n_{NLr} and n_{NLi} are the real and imaginary part of the nonlinear refractive index, respectively, while the n_{Lr} and n_{Li} are the real and imaginary part of the linear refractive index. These four quantities can be calculated from Eq. (7) and (8):

$$n_{Lr} = \sqrt{\frac{|\varepsilon_L| + |\varepsilon_{Lr}|}{2}}, \quad n_{NLr} = \sqrt{\frac{|\varepsilon_{NL}| + |\varepsilon_{NLr}|}{2}} \tag{7}$$

$$n_{Li} = \sqrt{\frac{|\varepsilon_L| - |\varepsilon_{Lr}|}{2}}, \quad n_{NLi} = \sqrt{\frac{|\varepsilon_{NL}| - |\varepsilon_{NLr}|}{2}} \tag{8}$$

3. Key findings and discussion

The $\chi_r^{(3)}$ extracted from our experiments is almost 6 times higher than that of the non-degenerate case [17], with values up to 3.5 × 10^{-19} m^2/V^2, while the $\chi_i^{(3)}$ changes sign and becomes negative. Figure 3(a) and 3(b) show Δn_r and Δn_i as a function of both I_{pump} and wavelength, respectively. We observe that the maximum change of the refractive index, corresponding to the highest pump intensity, is shifted in wavelength of about 80 nm with respect to the maximum change Δn_r induced by the lowest I_{pump}. This spectral shift is understood to be due to the shift in the ENZ wavelength due to the redistribution of electrons in the conduction band caused by the intraband excitation [32].

In this work, the maximum value of the n_{2r} was measured to be 5.17 × 10^{-12} cm^2/W at 1311 nm, about 13 times larger than the value measured in the non-degenerate case. On the other hand, the measured β_2 was found to be negative in sign and monotonically decreasing for increasing values of wavelength.

Optical Materials EXPRESS

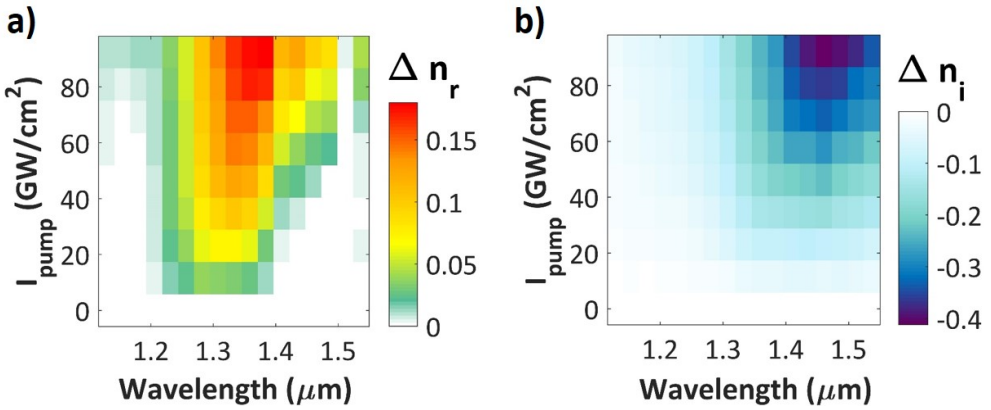

Fig. 3. Variation of the real (a) and imaginary (b) part of the refractive index Δn_r and Δn_i, respectively, as a function of both pump/probe wavelength and the incident pump intensity I_{pump}.

For operational purposes, it is useful to report both the minimum of β_2 and its value at the wavelength of maximum n_{2r}, which are $\beta_2 = -1.4 \times 10^{-6}$ cm/W (at 1449 nm, wavelength of minimum β_2) and $\beta_2 = -7.1 \times 10^{-7}$ cm/W (at 1311nm, wavelength of maximum n_{2r}), respectively. This prove that for an opportune choice of the operational wavelength, the degenerate configuration allows for considerably enhanced nonlinearities or efficient ultra-fast saturable absorption [33]. In addition, because the peak of Δn_r is separated from the dip of Δn_i by a large wavelength distance (~100 nm), AZO thin films could be exploited for efficient ultra-fast modulation of optical signals in either amplitude or phase. Moreover, it is worth noting that a Δn_r of about 0.17 was obtained for a I_{pump} of 90 GW/cm^2 at around 1350 nm, whereas in the non-degenerate case the same Δn_r were observed at the same wavelength for a I_{pump} of 400 GW/cm^2 [17].

The very high nonlinearities reported in the present manuscript can also be used to manipulate the spectral properties of optical pulses [17,19,32,34,35] and for applications in ultrafast beam steering and wavefront shaping [36,37]. Finally, the same system can produce highly efficient four-wave mixing, as already shown by Vezzoli and associates [21] or used as an active medium in dynamic nanocavities [38].

4. Conclusion

In conclusion, the present paper puts into context the emerging field of TCO-based plasmonics starting from material considerations and taking into account few among the most important recent achievements towards metal-free nanophotonics. We report our recent study of ultra-fast optical nonlinearities in AZO thin films probed at ENZ wavelengths and driven by degenerate optical excitation. It is important to underline that the strategy presented in this paper differs from the approach reported in [17], because the nonlinear response of the degenerate case is mediated also by an increased third-order susceptibility. Our experimental conditions are effective in enhancing the nonlinear Kerr coefficient by over one order of magnitude and the third-order nonlinear susceptibility by 6 times when making a comparison with the non-degenerate pumping scheme. The largest induced changes in the real and imaginary refractive index have a wavelength separation of about 100 nm. This creates two well defined operational wavelengths which can allow for efficient modulation of the optical signal operated on either the amplitude or the phase of the propagating radiation. Our observations make the degenerate nonlinearities of AZO thin films suitable for various applications, ranging from the design of nanophotonics devices to the study of the fundamental physics in time-varying media. *Relevant data can be accessed at* [39] *under ODC-By license*.

Optical Materials EXPRESS

Funding

M.F. acknowledges support from EPSRC (UK, Grant EP/P019994/1) and from The Royal Society (Project num.: RG2017R1). M.C. acknowledges support from EPSRC and Innovate UK (UK, Grant EP/S001573/1, EP/R043299/1), C.D., A.B., V.M.S. acknowledge support from the U.S. Department of Energy, Office of Basic Energy Sciences, Division of Materials Sciences and Engineering under Award DE-SC0017717 (C.D., Sample Fabrication) and support from Air Force Office of Scientific Research (AFOSR) Grant No. FA9550-18-1-0002". D.F. acknowledges financial support from EPSRC (UK, Grant No. EP/M009122/1).

References

1. D. G. Baranov, D. A. Zuev, S. I. Lepeshov, O. V. Kotov, A. E. Krasnok, A. B. Evlyukhin, and B. N. Chichkov, "All-dielectric nanophotonics: the quest for better materials and fabrication techniques," Optica **4**(7), 814–825 (2017).
2. I. Staude and J. Schilling, "Metamaterial-inspired silicon nanophotonics," Nat. Photonics **11**(5), 274–284 (2017).
3. S. Liu, M. B. Sinclair, S. Saravi, G. A. Keeler, Y. Yang, J. Reno, G. M. Peake, F. Setzpfandt, I. Staude, T. Pertsch, and I. Brener, "Resonantly Enhanced Second-Harmonic Generation Using III-V Semiconductor All-Dielectric Metasurfaces," Nano Lett. **16**(9), 5426–5432 (2016).
4. Z Yue, B. Cai, L. Wang, X. Wang, and M. Gu, "Intrinsically core-shell plasmonic dielectric nanostructures with ultrahigh refractive index," Sci. Adv. **2**, 1501536 (2016).
5. G. Kang, J. Yoo, J. Ahn, and K. Kim, "Transparent dielectric nanostructures for efficient light management in optoelectronic applications," Nano Today **10**(1), 22–47 (2015).
6. M. R. Shcherbakov, S. Liu, V. V. Zubyuk, A. Vaskin, P. P. Vabishchevich, G. Keeler, T. Pertsch, T. V. Dolgova, I. Staude, I. Brener, and A. A. Fedyanin, "Ultrafast all-optical tuning of direct-gap semiconductor metasurfaces," Nat. Commun. **8**(1), 17 (2017).
7. J. Kim, S. Choudhury, C. DeVault, Y. Zhao, A. V. Kildishev, V. M. Shalaev, A. Alù, and A. Boltasseva, "Controlling the Polarization State of Light with Plasmonic Metal Oxide Metasurface," ACS Nano **10**(10), 9326–9333 (2016).
8. P. Guo, R. P. H. Chang, and R. D. Schaller, "Transient negative optical nonlinearity of indium oxide nanorods arrays in the full-visible range," ACS Photonics **4**(6), 1494–1500 (2017).
9. P. Guo, R. D. Schaller, J. B. Ketterson, and R. P. H. Chang, "Ultrafast switching of tunable infrared plasmons in indium tin oxide nanorod arrays with large absolute amplitude," Nat. Photonics **10**(4), 267–273 (2016).
10. M. Abb, P. Albella, J. Aizpurua, and O. L. Muskens, "All-Optical Control of a Single Plasmonic Nanoantenna-ITO Hybrid," Nano Lett. **11**(6), 2457–2463 (2011).
11. M. Abb, Y. Wang, C. H. de Groot, and O. L. Muskens, "Hotspot-mediated ultrafast nonlinear control of multifrequency plasmonic nanoantennas," Nat. Commun. **5**(1), 4869 (2014).
12. I. Liberal and N. Engheta, "Near-zero refractive index photonics," Nat. Photonics **11**(3), 149–158 (2017).
13. X. Niu, X. Hu, S. Chu, and Q. Gong, "Epsilon-Near-Zero Photonics: A New Platform for Integrated Devices," Adv. Opt. Mater. **6**(10), 1701292 (2018).
14. O. Reshef, E. Giese, M. Zahirul Alam, I. De Leon, J. Upham, and R. W. Boyd, "Beyond the perturbative description of the nonlinear optical response of low-index materials," Opt. Lett. **42**(16), 3225–3228 (2017).
15. N. Kinsey, C. DeVault, J. Kim, M. Ferrera, V. M. Shalaev, and A. Boltasseva, "Epsilon-near-zero Al-doped ZnO for ultrafast switching at telecom wavelengths," Optica **2**(7), 616–622 (2015).
16. A. M. Urbas, Z. Jacob, L. Dal Negro, N. Engheta, A. D. Boardman, P. Egan, A. B. Khanikaev, V. Menon, M. Ferrera, N. Kinsey, C. DeVault, J. Kim, V. M. Shalaev, A. Boltasseva, J. Valentine, C. Pfeiffer, A. Grbic, E. Narimanov, L. Zhu, S. Fan, A. Alù, E. Poutrina, N. M. Litchinitser, M. A. Noginov, K. F. Macdonald, E. Plum, X. Liu, P. F. Nealey, C. R. Kagan, C. B. Murray, D. A. Pawlak, I. I. Smolyaninov, V. N. Smolyaninova, and D. Chanda, "Roadmap on optical metamaterials," J. Opt. **18**(9), 093005 (2016).
17. L. Caspani, R. P. M. Kaipurath, M. Clerici, M. Ferrera, T. Roger, J. Kim, N. Kinsey, M. Pietrzyk, A. Di Falco, V. M. Shalaev, A. Boltasseva, and D. Faccio, "Enhanced nonlinear refractive index in ε-near-zero materials," Phys. Rev. Lett. **116**(23), 233901 (2016).
18. M. Z. Alam, I. De Leon, and R. W. Boyd, "Large optical nonlinearity of indium tin oxide in its epsilon-near-zero region," Science **352**(6287), 795–797 (2016).
19. M. Clerici, N. Kinsey, C. DeVault, J. Kim, E. G. Carnemolla, L. Caspani, A. Shaltout, D. Faccio, V. Shalaev, A. Boltasseva, and M. Ferrera, "Controlling hybrid nonlinearities in transparent conducting oxides via two-colour excitation," Nat. Commun. **8**, 15829 (2017).
20. A. Capretti, Y. Wang, N. Engheta, and L. Dal Negro, "Enhanced third-harmonic generation in Si-compatible epsilon-near-zero indium tin oxide nanolayers," Opt. Lett. **40**(7), 1500–1503 (2015).
21. S. Vezzoli, V. Bruno, C. DeVault, T. Roger, V. M. Shalaev, A. Boltasseva, M. Ferrera, M. Clerici, A. Dubietis, and D. Faccio, "Optical Time Reversal from Time-Dependent Epsilon-Near-Zero Media," Phys. Rev. Lett. **120**(4), 043902 (2018).
22. M. Z. Alam, S. A. Schulz, J. Upham, I. De Leon and R. W. Boyd, "Unity-order nonlinear index change in a metasurface", Proc. Photonics North 2017, 255-wx55–265 (2017).

Optical Materials EXPRESS

23. M. Z. Alam, S. A. Schulz, J. Upham, I. De Leon, and R. W. Boyd, "Large optical nonlinearity of nanoantennas coupled to an epsilon-near-zero material," Nat. Photonics **12**(2), 79–83 (2018).
24. R. W. Boyd, *Nonlinear Optics,* 3rd ed. (Elsevier, 2008).
25. E. M. Vogel, M. J. Weber, and D. M. Krol, "Nonlinear optical phenomena in glass," Phys. Chem. Glasses **32**(6), 231–254 (1991).
26. C. C. Wang, "Empirical Relation between the Linear and the Third-order Nonlinear Optical Susceptibilities," Phys. Rev. B **2**(6), 2045–2048 (1970).
27. R. C. Miller, "Optical second harmonic generation in piezoelectric crystals," Appl. Phys. Lett. **5**(1), 17–19 (1964).
28. G. V. Naik, J. Liu, A. V. Kildishev, V. M. Shalaev, and A. Boltasseva, "Demonstration of Al:ZnO as a plasmonic component for near-infrared metamaterials," Proc. Natl. Acad. Sci. U.S.A. **109**(23), 8834–8838 (2012).
29. A. V. Singh, R. M. Mehra, N. Buthrath, A. Wakahara, and A. Yoshida, "Highly conductive and transparent aluminum-doped zinc oxide thin films prepared by pulsed laser deposition in oxygen ambient," J. Appl. Phys. **90**(11), 5661–5665 (2001).
30. H. Kim, J. Horwitz, S. Qadri, and D. Chrisey, "Epitaxial growth of Al-doped ZnO thin films grown by pulsed laser deposition," Thin Solid Films **420–421**, 107–111 (2002).
31. R. M. Kaipurath, M. Pietrzyk, L. Caspani, T. Roger, M. Clerici, C. Rizza, A. Ciattoni, A. Di Falco, and D. Faccio, "Optically induced metal-to-dielectric transition in Epsilon-Near-Zero metamaterials," Sci. Rep. **6**(1), 27700 (2016).
32. P. Kelly and L. Kuznetsova, "Pulse shaping in the presence of enormous second-order dispersion in Al:ZnO/ZnO epsilon-near-zero metamaterial," Appl. Phys. B **124**(4), 60 (2018).
33. J. Guo, H. Zhang, C. Zhang, Z. Li, Y. Sheng, C. Li, X. Bao, B. Man, Y. Jiao, and S. Jiang, "Indium tin oxide nanocrystals as saturable absorbers for passively Q-switched erbium-doped fiber laser," Opt. Mater. Express **7**(10), 3494–3502 (2017).
34. M. Ferrera and E. G. Carnemolla, "Ultra-fast transient plasmonics using transparent conductive oxides," J. Opt. **20**(2), 024007 (2018).
35. A. Shaltout, A. Kildishev, and V. Shalaev, "Time-varying metasurfaces and Lorentz non-reciprocity," Opt. Mater. Express **5**(11), 2459–2467 (2015).
36. S. B. Raghunathan, H. F. Schouten, W. Ubachs, B. E. Kim, C. H. Gan, and T. D. Visser, "Dynamic beam steering from a subwavelength slit by selective excitation of guided modes," Phys. Rev. Lett. **111**(15), 153901 (2013).
37. H. Frostig, E. Small, A. Daniel, P. Oulevey, S. Derevyanko, and Y. Silberberg, "Focusing light by wavefront shaping through disorder and nonlinearity," Optica **4**(9), 1073–1079 (2017).
38. J. Kim, E. G. Carnemolla, C. DeVault, A. M. Shaltout, D. Faccio, V. M. Shalaev, A. V. Kildishev, M. Ferrera, and A. Boltasseva, "Dynamic Control of Nanocavities with Tunable Metal Oxides," Nano Lett. **18**(2), 740–746 (2018).
39. DOI: 10.17861/f9701bb5-2534-4f91-bd25-2e605b22e0f0